ICAS-98-2,6,4

A98-31513

A TIME MARCHING, TYPE-DEPENDENT, FINITE DIFFERENCE ALGORITHM FOR THE MODIFIED TRANSONIC SMALL DISTURBANCE EQUATION

J.A. Gear, E. Ly & N.J.T. Phillips

Department of Mathematics, RMIT University, Melbourne, Victoria 3001, Australia.

Abstract

A new time marching finite difference algorithm is formulated for the solution of the Modified Transonic Small Disturbance Equation. The algorithm determines the unsteady reduced velocity potential and pressure coefficient on the bounding surface of a wing. Unsteady transonic flow calculations are presented for the flow over a large aspect ratio rectangular wing of unit chord length and for the flow over a swept and tapered wing.

Introduction

A new time marching finite difference algorithm is formulated for the solution of the modified Transonic Small Disturbance (TSD) equation.[8] The approximate factorization technique was first developed for the Full-Potential Equation and was shown to be very robust for either steady or oscillatory transonic flow calculations.[10] The TSD equation was first solved using the approximate factorization method by Batina.[2, 3]

Initially a time accurate finite difference discretization is constructed. The reduced potential is determined via a Newton linearization of the finite difference scheme. In the iterative technique the coefficient matrix acting on the unknown potential difference is approximately factored and the potential determined via the solution of three block diagonal linear systems. Two of which are block tridagonal. Each linear system can be solved by the LU factorization method. Due to the block structure of the linear systems the solution procedure is easily vectorized.

The finite difference scheme includes second order type-dependent differencing[3, 4, 7] for all streamwise derivatives. As the flow changes from subsonic to supersonic the type-dependent difference operators smoothly change from central difference approximations to backward difference approximations. This ensures a smooth transition from subsonic to supersonic flow. Hence entropy violating[4] decompression shock discontinuities will not develop. As the flow changes from supersonic to subsonic the type-dependent operator changes to an appropriate shock point operator.[9] Thus ensuring a sharp shock profile. Note that the type-dependent differencing operators have been modified to produce sharper shock profiles with little overshoot (after the shock).

Nonreflective boundary conditions[6] are used at the far field boundaries and a shearing transformation[5, 8] is employed so that any given wing can be mapped into a rectangular region.

The modified TSD equation for the reduced potential,[2] may be written as

$$M^2\frac{\partial}{\partial t}(\phi_t + 2\phi_x) + \frac{\beta^2}{2\bar{u}}\frac{\partial}{\partial x}(\phi_x - \bar{u})^2 - \frac{\partial}{\partial y}\phi_y - \frac{\partial}{\partial z}\phi_z = G\frac{\partial}{\partial x}\phi_y^2 + H\frac{\partial}{\partial y}(\phi_x\phi_y). \quad (1)$$

The constants β, $\bar{u}$, G and H are given by

$$\beta^2 = 1 - M^2,$$
$$\bar{u} = \frac{\beta^2}{M^2(1+\gamma)},$$
$$G = M^2(\gamma - 3)/2,$$
$$H = (1-\gamma)M^2.$$

Here x, y and z represents a nondimensional rectangular Cartesian coordinate system, t is the time variable, γ is the ratio of specific heats, M is the freestream Mach number and in nondimensional terms the fluid velocity is given by $\mathbf{v} = \nabla(x + \phi)$. Equation (1) is locally of hyperbolic type representing supersonic flow for $\phi_x > \bar{u}$ and of elliptic type representing subsonic flow for $\phi_x < \bar{u}$.

The boundary conditions imposed upon the flow field are

$$\phi_x \pm \frac{M}{1 \pm M}\phi_t = 0 \quad \text{down/upstream boundary,} \quad (2)$$

$$\phi_z \pm \frac{M}{\beta}\phi_t = 0 \quad \text{above/below boundary,} \quad (3)$$

$$\phi_y + \frac{M}{\beta}\phi_t = 0 \quad \text{right spanwise boundary,} \quad (4)$$

$$\phi_y = 0 \quad \text{symmetry plane,} \quad (5)$$

$$\langle \phi_z \rangle = 0 \quad \text{wake,} \quad (6)$$

$$\langle \phi_x + \phi_t \rangle = 0 \quad \text{wake,} \quad (7)$$

where $\langle \bullet \rangle$ indicates the jump in the indicated quantity across the wake. If the upper/lower surface of the wing is defined as $z = h^{\pm}(x, y, t)$, then the wing flow tangency boundary condition is

$$\phi_z^{\pm} = h_x^{\pm} + h_t, \quad (8)$$

21st ICAS Congress
13-18 September 1998
Melbourne, Australia

which is imposed at the mean plane of the wing. The plus and minus superscript indicate the upper and lower wing surfaces, respectively.

The dependence of the solution on the wing mesh spacing poses a problem when applied to swept and tapered wings. Due to the large number of points required, it is impractical to maintain a sufficiently fine mesh spacing along the leading edge of a swept wing in a Cartesian coordinate system. To rectify this problem we map the wing into a rectangular region using a shearing transformation.[1, 8]

In the shearing transformation the far-field boundaries are kept independent of the wing planform and aligned with respect to the freestream direction, hence both the physical and computational domains are contained within rectangular regions. Smooth first and second derivatives occur for values of the metric quantities, particularly near boundaries and grid lines are clustered near the leading and trailing edges of the wing. In general terms the transformation is given by

$$\xi = \xi(x, y), \qquad \eta = y, \qquad \zeta = \zeta(z), \tag{9}$$

where ξ, η and ζ are the nondimensional computational coordinates in the x, y and z directions, respectively.

After applying the shearing transformation, Equation (1) can be written as

$$\begin{aligned}
&M^2\phi_{tt} + 2M^2 w_t + \frac{\beta^2}{2\bar{u}}\xi_x\frac{\partial}{\partial\xi}w^2 \\
&\quad - \frac{\partial}{\partial\eta}\phi_\eta - \zeta_z\frac{\partial}{\partial\zeta}\zeta_z\phi_\zeta \\
&= \frac{\partial}{\partial\eta}\xi_y\phi_\xi + \xi_y\frac{\partial}{\partial\xi}(\phi_\eta + \xi_y\phi_\xi) \\
&\quad + G\xi_x\frac{\partial}{\partial\xi}(\phi_\eta + \xi_y\phi_\xi)^2 \\
&\quad + H\left(\frac{\partial}{\partial\eta} + \xi_y\frac{\partial}{\partial\xi}\right)\left(\xi_x\phi_\xi(\phi_\eta + \xi_y\phi_\xi)\right) \\
&= P(\phi),
\end{aligned} \tag{10}$$

where $w = \xi_x\phi_\xi - \bar{u}$. Note that w is positive/negative when the flow is locally supersonic/subsonic.

Finite Difference Discretization and Solution Procedure

In the finite difference discretization of Equation (10) the time derivative terms ϕ_{tt} and w_t are approximated by second-order accurate backward finite difference formulas about the time level $t = (n+1)\Delta t$, where Δt is the time increment. That is

$$\begin{aligned}
&M^2(2\phi^{n+1} - 5\phi^n + 4\phi^{n-1} - \phi^{n-2}) \\
&\quad + M^2\Delta t(3w^{n+1} - 4w^n + w^{n-1}) \\
&\quad + \frac{\beta^2(\Delta t)^2}{2\bar{u}}\xi_x\frac{\partial}{\partial\xi}(w^{n+1})^2 - (\Delta t)^2\phi^{n+1}_{\eta\eta} \\
&\quad - (\Delta t)^2\zeta_z\frac{\partial}{\partial\zeta}(\zeta_z\phi_\zeta)^{n+1} - (\Delta t)^2 P(\phi^{n+1}) \\
&= R(\phi^{n+1}, \phi^n, \phi^{n-1}, \phi^{n-2}).
\end{aligned} \tag{11}$$

Here ϕ^{n+1} represents the unknown potential at time level $(n+1)\Delta t$. Our aim is to find ϕ^{n+1} at all points, given ϕ^n, ϕ^{n-1}, *etc.* Equation (11) is nonlinear so the solution is found by a Newton linearization procedure about ϕ^*, where ϕ^* is the current best estimate of ϕ^{n+1}. We substitute $\phi^{n+1} = \phi^* + \Delta\phi$ into the left hand side of Equation (11), linearize about $\Delta\phi$ and approximately factor the resulting expression,

$$\begin{aligned}
&\frac{-1}{2M^2}R(\phi^*, \phi^n, \phi^{n-1}, \phi^{n-2}) \\
&= \Delta\phi + \frac{3\Delta t}{2}\xi_x\frac{\partial}{\partial\xi}\Delta\phi + \frac{\beta^2(\Delta t)^2}{2M^2\bar{u}}\xi_x\frac{\partial}{\partial\xi}\xi_x w^*\frac{\partial}{\partial\xi}\Delta\phi \\
&\quad - \frac{(\Delta t)^2}{2M^2}\frac{\partial^2}{\partial\eta^2}\Delta\phi - \frac{(\Delta t)^2}{2M^2}\zeta_z\frac{\partial}{\partial\zeta}\zeta_z\frac{\partial}{\partial\zeta}\Delta\phi \\
&\approx L_\xi L_\eta L_\zeta\Delta\phi,
\end{aligned} \tag{12}$$

where

$$L_\xi = 1 + \frac{3\Delta t}{2}\xi_x\frac{\partial}{\partial\xi} + \frac{\beta^2(\Delta t)^2}{2M^2\bar{u}}\xi_x\frac{\partial}{\partial\xi}\xi_x w^*\frac{\partial}{\partial\xi} \tag{13}$$

$$L_\eta = 1 - \frac{(\Delta t)^2}{2M^2}\frac{\partial^2}{\partial\eta^2} \tag{14}$$

$$L_\zeta = 1 - \frac{(\Delta t)^2}{2M^2}\zeta_z\frac{\partial}{\partial\zeta}\zeta_z\frac{\partial}{\partial\zeta} \tag{15}$$

In Equation (12) higher order terms in $\Delta\phi$ have been ignored. Equation (12) forms a linear system which can be solved for $\Delta\phi$ at each point in the computational domain. During the convergence of the iteration procedure $\Delta\phi \to 0$ and the solution will be given by $\phi^{n+1} \approx \phi^*$. The factored scheme can be implemented as

$$L_\xi\Delta\phi'' = \frac{-1}{2M^2}R(\phi^*, \phi^n, \phi^{n-1}, \phi^{n-2}), \tag{16}$$

$$L_\eta\Delta\phi' = \Delta\phi'', \tag{17}$$

$$L_\zeta\Delta\phi = \Delta\phi'. \tag{18}$$

A new approximation to ϕ^{n+1} is found by systematically solving the system of Equations (16) for $\Delta\phi''$, Equations (17) for $\Delta\phi'$ and Equations (18) for $\Delta\phi$. The factorization is constructed so that the coefficient matrix in the system of Equations (16) contains the terms due the dominant ξ-derivatives and consequently forms a block diagonal linear system. Similarly the coefficient matrix in the system of Equations (17) and (18) contain the terms

due the dominant $\eta-$ and $\zeta-$ derivatives. Consequently the systems (17) and (18) can be reordered to produce block tridiagonal systems.

Central difference formulae are employed for all the $\eta-$ and $\zeta-$ derivatives. The $\xi-$ derivative terms must be approximated using type-dependent mixed difference operators. The type-dependent differencing allows for a smooth transition from subsonic to supersonic flow.

The far-field boundaries are aligned with respect to the freestream and are midway between adjacent grid points. For the far-field boundary conditions, Equations (2) to (4), the time derivatives are approximated by second-order accurate backward finite difference formulas and central difference formulas are employed for all the spatial derivatives.

The symmetry condition, Equation (5), is imposed by requiring that $\phi_y = \phi_\eta + \xi_y \phi_\xi = 0$. Since ξ is odd with respect to the spanwise coordinate $\xi_y(0) = 0$ and hence at the root chord the imposed symmetry condition is $\phi_\eta = 0$.

The boundary conditions on the wing and the wake are imposed within the differencing of the $\zeta_z(\zeta_z\phi_\zeta)_\zeta$ term, see Equation (10). The finite difference grid is constructed using a block structure with one block for the flow above the plane of the wing and the other for the flow below. In each block the wing lies mid-way between adjacent grid planes, with one plane of grid points representing an artificial level inside the wing. After each sweep through Equations (16) to (18) information is exchanged between the blocks and the wing plane boundary conditions are satisfied.

Initially a steady-state solution is calculated[5, 6] and the steady reduced potential is used as an initial starting state for the unsteady calculation. At each new time level $(t = (n+1)\Delta t)$ an estimate of the reduced potential is required to start the iteration procedure. This estimate is provided by performing a time linearization about level $t = n\Delta t$. That is, initially $\phi^{n+1} = \phi^n + \Delta\phi$.

Type-Dependent Differencing

Type-Dependent differencing is used in transonic flow computation to reflect the change in nature of the equation between regions of subsonic and supersonic flow. That is, differenct finite difference formulae are used in different flow regions. In the supersonic region we would expect to be using backward, or so called upwind differencing, and in the subsonic region central differencing.

The reduced potential, $\phi(\xi, \eta, \zeta)$, is defined at the grid points (ξ_i, η_j, ζ_k), and $w = \xi_x\phi_\xi - \bar{u}$ is found using central differences about half grid points in space. That is

$$w_{i+1/2} = (\xi_x)_{i+1/2}\frac{\phi_{i+1} - \phi_i}{\Delta\xi} - \bar{u}.$$

In the differencing of terms like $\partial(w^2)/\partial\xi$ the w values are deemed either to be supersonic or subsonic and are accordingly used for either central or backward differencing. Variables $\tilde{w}$ and $\hat{w}$ are defined so that $\tilde{w}$ is defined as w in the subsonic region and zero in the supersonic region, and $\hat{w}$ is defined as w in the supersonic region and zero in the subsonic region. That is

$$\begin{aligned} \tilde{w}_{i+1/2} &= (1 - \epsilon_{i+1/2})\, w_{i+1/2}, \\ \hat{w}_{i+1/2} &= \epsilon_{i+1/2} w_{i+1/2}, \end{aligned} \tag{19}$$

where

$$\epsilon_{i-1/2} = \begin{cases} 1 & \text{for } w_{i-1/2} \geq 0 \\ 0 & \text{for } w_{i-1/2} < 0 \end{cases}. \tag{20}$$

The differencing for the $(w^2)_\xi$ term uses the $\tilde{w}$ variable for central differencing and the $\dot{w}$ variable for backward differencing. A second-order type-dependent differencing scheme for $(w^2)_\xi$ is given by[2, 3, 4, 5, 6]

$$\left.\frac{\partial}{\partial\xi}w^2\right|_i \approx \overrightarrow{\Delta}\tilde{w}^2_{i-1/2} + \overleftarrow{\Delta}\hat{w}^2_{i-1/2} + \Delta\xi\overleftarrow{\Delta}(\epsilon_{i-1/2}\overleftarrow{\Delta}\hat{w}^2_{i-1/2}), \tag{21}$$

where $\overrightarrow{\Delta}/\overleftarrow{\Delta}$ is the forward/backward difference operator. For example

$$\overrightarrow{\Delta}w_{i-1/2} = \frac{w_{i+1/2} - w_{i-1/2}}{\Delta\xi}.$$

Notice that in the subsonic/supersonic region a central/backward difference approximation is used.

As the flow changes from subsonic to supersonic the differencing changes from central to upwind differencing, in a smooth way, without differencing across the sonic line. This ensures that expansion shocks will not develop.[4] As the flow changes from supersonic to subsonic then the differencing changes to an appropriate shock point operator.[9] For example if $\epsilon_{i+1/2} = 0$ and $\epsilon_{i-1/2} = \epsilon_{i-3/2} = \epsilon_{i-5/2} = 1$ then

$$\Delta\xi\left.(w^2)_\xi\right|_i \approx \left(w^2_{i+1/2} - 0\right) + \left(2w^2_{i-1/2} - 3w^2_{i-3/2} + w^2_{i-5/2}\right), \tag{22}$$

both a central and an upwind difference. Note here that 0 is the sonic reference value for w. If $\epsilon_{i+1/2} = \epsilon_{i-1/2} = 0$ and $\epsilon_{i-3/2} = \epsilon_{i-5/2} = 1$, essentially a subsonic point, then

$$\Delta\xi\left.(w^2)_\xi\right|_i \approx \left(w^2_{i+1/2} - w^2_{i-1/2}\right) + \left(0 - 2w^2_{i-3/2} + w^2_{i-5/2}\right). \tag{23}$$

Unfortunately the combination of Equations (22) and (23) tends to spread the shock discontinuity over several grid spaces.

A new type-dependent differencing method is proposed that should produce a sharper shock profile and still eliminate expansion shocks. In the neighborhood of the sonic line the new scheme is equivalent to Equation (21). Hence expansion shocks are eliminated. The modified type dependent differencing is,

$$\frac{\partial}{\partial\xi}w^2|_i \approx \overrightarrow{\Delta}\tilde{w}^2_{i-1/2} + \epsilon_{i-1/2}[\overleftarrow{\Delta}\hat{w}^2_{i-1/2} + \Delta\xi\overleftarrow{\Delta}(\epsilon_{i-1/2}\overleftarrow{\Delta}\hat{w}^2_{i-1/2})], \quad (24)$$

where $\tilde{w}$ and $\hat{w}$ are defined by Equation (19) and ϵ by Equation (20). Notice now that if $\epsilon_{i+1/2} = \epsilon_{i-1/2} = 0$ and $\epsilon_{i-3/2} = \epsilon_{i-5/2} = 1$ then

$$\Delta\xi\,(w^2)_\xi\,|_i \approx w^2_{i+1/2} - w^2_{i-1/2}$$

a central difference approximation. The reader should compare this with Equation (23).

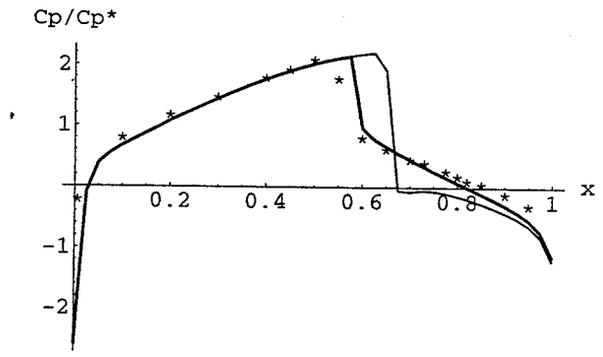

FIGURE 1: Comparison between the type-dependent differencing scheme, Equation (21) (thin line), modified scheme, Equation (24) (thick line) and experimental data (*) for two-dimensional flow over a NACA64A006 airfoil.

Figure 1 shows a comparison of experimentally measured[11] and numerical estimates of the steady pressure coefficient on the surface of a NACA64A006 airfoil at $0°$ angle of attack, and $M = 0.875$. Numerical results were obtained using the type-dependent differencing scheme, Equation (21) and the modified scheme, Equation (24). Notice that the modified scheme produces a sharper shock profile, there is an absence of overshoot after the shock and the shock position is much more accurately determined.

In the differencing of $\frac{\partial}{\partial\xi}(\xi_x w\frac{\partial}{\partial\xi}\Delta\phi'')$ which appears on the left hand side of Equation (16), the following first-order mixed difference operator is used,

$$\frac{\partial}{\partial\xi}f\Big|_i = \overrightarrow{\Delta}\tilde{f}_{i-1/2} + \epsilon_{i-1/2}\overleftarrow{\Delta}\hat{f}_{i-1/2}, \quad (25)$$

where

$$f = \xi_x w\frac{\partial\Delta\phi''}{\partial\xi},$$
$$\hat{f}_{i+1/2} = \epsilon_{i+1/2}f_{i+1/2},$$
$$\tilde{f}_{i+1/2} = (1-\epsilon_{i+1/2})f_{i+1/2}.$$

In using the first-order mixed difference operator Equation (25) we decrease the bandwidth of the coefficient matrix in the system of Equations (16) from three to two, and hence speed up the solution procedure. Note that the scheme is still second-order as the corresponding terms in the residual R (see Equations (11) and (16)) are evaluated using the second-order mixed difference operator, Equation (24).

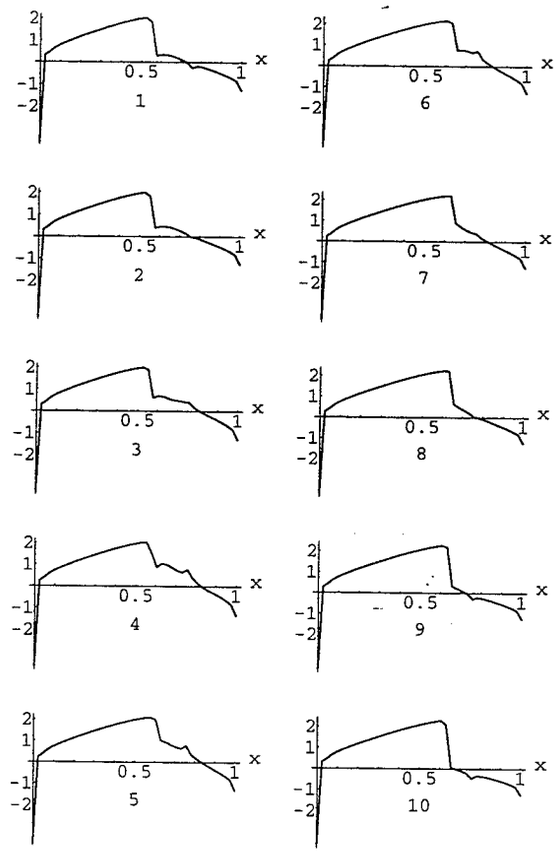

FIGURE 2: Scaled pressure coefficient (C_p/C_p^*) on the upper surface of the rectangular wing at the root section, with an oscillating quarter-chord flap. $M = 0.875$, reduced frequency $k = 0.235$ and $\Delta t = 0.01337$. The flap oscillates through one complete cycle.

In the evaluation of the residual R (see Equation (11)) if the terms w_i^{n+1}, w_i^n and w_i^{n-1} are evaluated like $w_i = (w_{i+1/2} + w_{i-1/2})/2$ (a central average), then the resulting numerical scheme is unstable. Note previously[2, 3, 6] the terms w_i^{n+1}, w_i^n, w_i^{n-1}

and $\partial(\Delta\phi)/\partial\xi$ were approximated using first-order upwind differences. In this new scheme the terms w_i and $\partial(\Delta\phi)/\partial\xi$ (see Equations (11) and (16)) are evaluated using a mixed difference operator that uses an upwind approximation in supersonic regions and a central approximation in subsonic regions. As the flow changes from subsonic to supersonic the mixed difference operator must change smoothly from the central approximation to the upwind approximation. Appropriate first and second-order mixed difference operators are respectively,

$$g_i = (\tilde{g}_{i-1/2} + \tilde{g}_{i+1/2})/2 + \hat{g}_{i-1/2}, \qquad (26)$$

$$g_i = (\tilde{g}_{i-1/2} + \tilde{g}_{i+1/2})/2 + \hat{g}_{i-1/2} + \epsilon_{i-1/2}(\hat{g}_{i-1/2} - \hat{g}_{i-3/2})/2, \qquad (27)$$

where $\hat{g}_{i+1/2} = \epsilon_{i+1/2} g_{i+1/2}$, and $\tilde{g}_{i+1/2} = (1 - \epsilon_{i+1/2}) g_{i+1/2}$. In the approximation of w_i, $g = w$ and the second-order approximation (Equation (27)) is used. In the evaluation of $\partial(\Delta\phi'')/\partial\xi|_i$, (see Equations (16) and (13)), $g = \partial(\Delta\phi)/\partial\xi$, and the first-order approximation (Equation (26)) is used.

Results

Calculations were performed for the flow over a large aspect ratio, rectangular wing of unit chord length and semi-span length 3. The airfoil cross section is a symmetric NACA64A006 section with a flap over the final 25% of the chord. The flap is allowed to oscillate with a maximum amplitude of 1°. Figures 2 and 3 show the scaled pressure coefficient (C_p/C_p^*) versus chord on the upper side of the wing at the root chord, at even time intervals over a complete cycle. The pressure coefficient, $C_p = -2(\phi_x + \phi_t)$, has been scaled with the critical pressure coefficient; $C_p^* = -2\bar{u}$. Values of C_p/C_p^* greater than one indicate locally supersonic flow. The reduced frequency, k, is a nondimensional frequency. In Figures 2 and 3 the position of the flap hinge can clearly be seen as a slight peak in the pressure profile. In Figure 2 the shock discontinuity is seen to oscillate between about $x = 0.58$ and $x = 0.65$ as the flap oscillates through a complete cycle. In Figure 3, initially when the flap is at 0° angle of attack (graph 1), there is no supersonic region. As the flap angle increases a supersonic region and a shock develop. As the flap angle returns to zero the shock begins to move forward. As the shock moves forward it loses strength and eventually moves off the wing.

Calculations were also performed for the flow over a swept and tapered wing at a freestream Mach number 0.9. The semispan length is 1 and the chord length is 1 (root chord) and tapers down to 0.2875 at the wing tip. The leading edge is given by $x = 0.625y$ and the trailing edge by $x = 1 - 0.0875y$. The airfoil cross section is a symmetric NACA65A004.8 section. The wing oscillates about $x = 0.5$ with an amplitude of 1° and a reduced frequency $k = 0.2$. Figure 4 shows the scaled pressure coefficient (C_p/C_p^*) on the upper surface when the wing is at 0° and 1° angle of attack. A clearly defined three-dimensional shock structure can be seen. Notice that the strength of the shock increases as the angle of attack increases. Figure 5 shows the scaled pressure coefficient at the wing root and tip sections when the wing is at 0° and 1° angle of attack. At 0° angle of attack there is no supersonic region at the wing root section, but as the angle of attack increases a supersonic region and shock develop. At the wing tip, as the angle of attack increases, the shock increases in strength and moves aft from about $x = 0.78$ to 0.83.

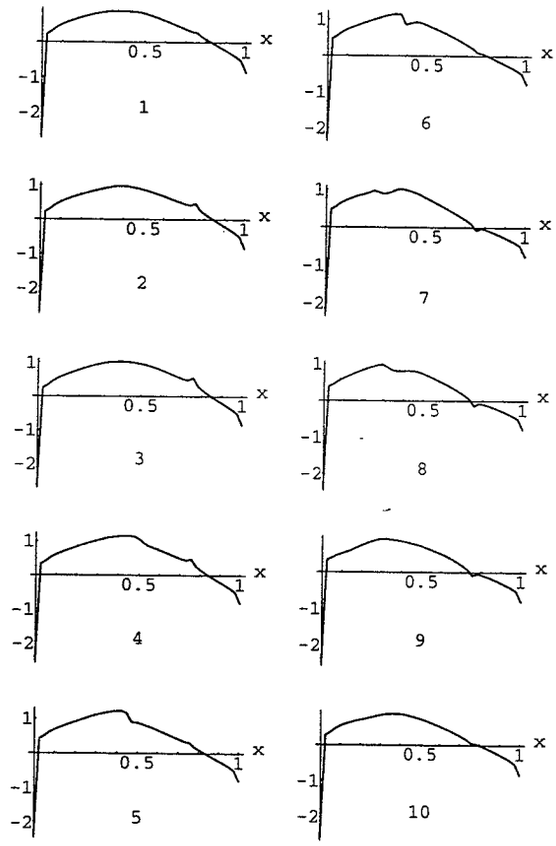

FIGURE 3: Scaled pressure coefficient (C_p/C_p^*) on the upper surface of the rectangular wing at the root section, with an oscillating quarter-chord flap, $M = 0.835$, reduced frequency $k = 0.248$ and $\Delta t = 0.01267$. The flap oscillates through one complete cycle.

Acknowledgement

This research was supported by a grant from the Defence Science and Technology Organization, Melbourne, Australia.

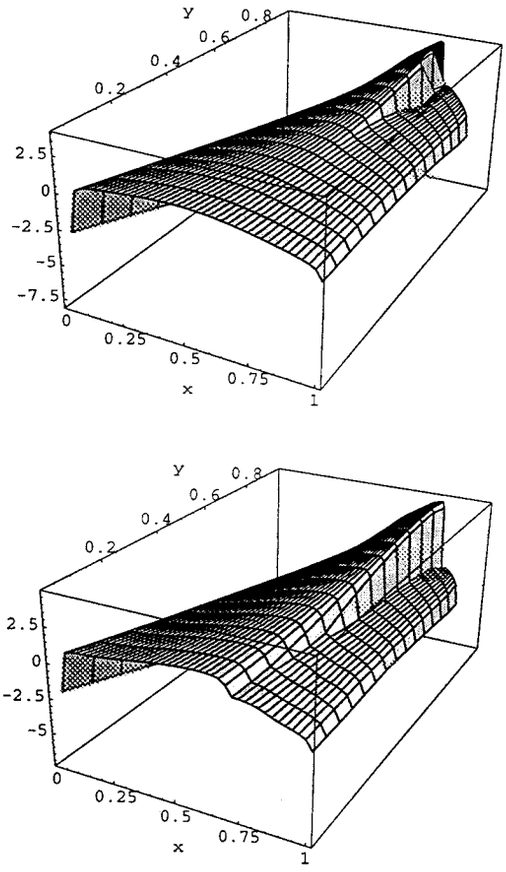

FIGURE 4: Scaled pressure coefficient (C_p/C_p^*) on the upper surface of the pitching tapered wing, when the wing is at 0° (top) and 1° (bottom) angle of attack.

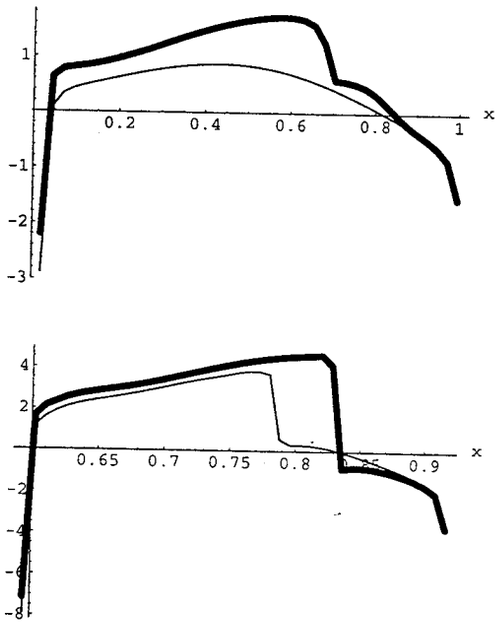

FIGURE 5: Scaled pressure coefficient (C_p/C_p^*) on the upper surface of the pitching tapered wing at the root (top) and tip chord (bottom) sections when the wing is at 0° (thin line) and 1° (thick line) angle of attack.

References

[1] Ballhaus, W. F., and Bailey, F. R. Numerical Calculation of Transonic Flow About Swept Wings. AIAA paper-72-677, 1972.

[2] Batina, J. T. Efficient Algorithm for Solution of the Unsteady Transonic Small-Disturbance Equation. *J. Aircraft 25*, 1988, 598–605.

[3] Batina, J. T. Unsteady Transonic Algorithm Improvements for Realistic Aircraft Applications. *J. Aircraft 26*, 1989, 131–139.

[4] Engquist, B., and Osher, S. Stable and Entropy Satisfying Approximations for Transonic Flow Calculations. *Mathematics of Computation 34*, 1980, 45–75.

[5] Gear, J. A. Approximate Factorization Algorithm for the Steady Transonic Small Disturbance Equation. *PICAST 2 -AAC 6, Second Pacific International Conference on Aerospace Science and Technology/Sixth Australian Aeronautical Conference.* (1995), The Institution of Engineers, Australia, pp. 911–916.

[6] Gear, J. A., and Polanco, F. G. An Approximate Factorization Algorithm for the Unsteady Transonic Small Disturbance Equation. *Computational Techniques and Application: CTAC95* (1996), R. L. May and A. K. Easton, editors, World Scientific, Singapore, pp. 335–342.

[7] Goorjian, P. M., and van Buskirk, R. Second-Order-Accurate Spatial Differencing for the Transonic Small-Disturbance Equation. *AIAA J. 23*, 1985, 1693–1699.

[8] Guruswamy, G. P., and Goorjian, P. M. An Efficient Coordinate Transformation Technique for Unsteady, Transonic Aerodynamic Analysis of Low Aspect-Ratio Wings. AIAA paper-84-0872, 1984.

[9] Murman, E. M. Analysis of Embedded Shock Waves Calculated by Relaxation Methods. *AIAA J. 12*, 1974, 626–633.

[10] Shankar, V., and Ide, H. Treatment of Steady and Unsteady Flows Using a Fast, Time-Accurate Unsteady Full-Potential Scheme. AIAA paper-85-4060, 1985.

[11] Tijdeman, H. Investigations of the Transonic Flow Around Oscillating Airfoils. Tech. rep., National Aerospace Lab. (NLR), Netherlands, 1977.